

# Absolute clock synchronization with a single time-correlated photon pair source over a 10 km optical fibre

JIANWEI LEE,<sup>1</sup> LIJIONG SHEN,<sup>1</sup> ADRIAN NUGRAHA UTAMA,<sup>1</sup> AND CHRISTIAN KURTSIEFER<sup>1,2,\*</sup>

<sup>1</sup>Centre for Quantum Technologies, National University of Singapore, 3 Science Drive 2, Singapore 117543, Singapore

<sup>2</sup>Department of Physics, National University of Singapore, 2 Science Drive 3, Singapore 117551, Singapore  
\*christian.kurtsiefer@gmail.com

**Abstract:** We demonstrate a point-to-point clock synchronization protocol based on bidirectionally propagating photons generated in a single spontaneous parametric down-conversion (SPDC) source. Tight timing correlations between photon pairs are used to determine the single and round-trip times measured by two separate clocks, providing sufficient information for distance-independent absolute synchronization secure against symmetric delay attacks. We show that the coincidence signature useful for determining the round-trip time of a synchronization channel, established using a 10 km telecommunications fiber, can be derived from photons reflected off the end face of the fiber without additional optics. Our technique allows the synchronization of multiple clocks with a single reference clock co-located with the source, without requiring additional pair sources, in a client-server configuration suitable for synchronizing a network of clocks.

© 2022 Optical Society of America

## 1. Introduction

Complementary to clock recovery schemes from data streams, absolute clock synchronization protocols, e.g. network time protocol (NTP), precision time protocol (PTP), two-way satellite time transfer (TWSTT), are widely-used to determine the offset between physically separated clocks [1–4]. By exchanging counter-propagating signals, and assuming a symmetric synchronization channel, parties estimate one-way propagation delays as half the round-trip time signals without characterizing their physical separation beforehand. Spatially separated parties then deduce their absolute clock offset by comparing signal propagation times measured with their devices with the expected propagation delay [5]. Recently, protocol implementations with entangled photon pairs suggest securing the synchronization channel by measuring non-local correlations – a technique inspired by entanglement-based quantum key distribution (QKD) [2, 6, 7] [6–8]. With independent hydrogen-maser and rubidium clocks as references, the protocol has a demonstrated timing stability limited to the intrinsic instability of the clocks over 7 km [9], and is secure against symmetric-delay attacks [6]. However, to realize a bidirectional exchange of photons, these demonstrations required a photon pair source at each end of the synchronization channel, posing a resource challenge when synchronizing multiple clocks.

In this work, we experimentally demonstrate a bidirectional clock synchronization protocol where the synchronization channel is established with a 10 km optical fiber and a single entangled photon pair source. The round-trip time is sampled using time-correlation measurements between the detection times of photon pairs, with one photon of the pair back-reflected at the remote side using the end face of the fiber. We demonstrate a distance-independent synchronization of two separated clocks, referenced to independent rubidium frequency standards. Already from a quite modest photon pair detection rate of  $160 \text{ s}^{-1}$  we obtain a precision sufficient to resolve clock

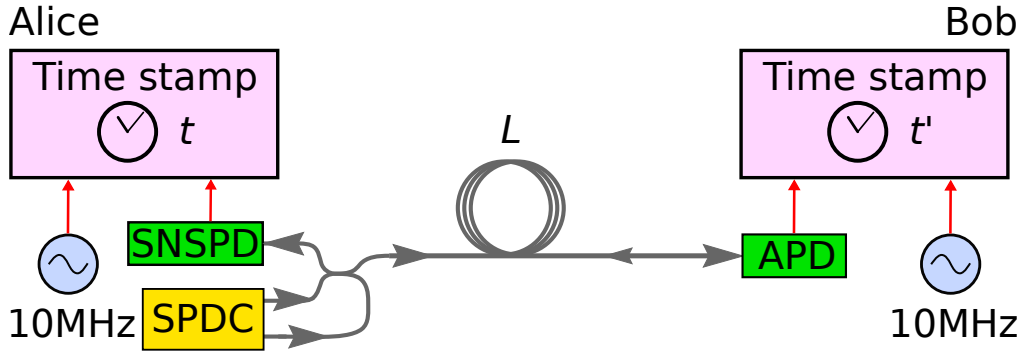


Fig. 1. Clock synchronization setup. Alice has a source of time-correlated photon pairs based on spontaneous parametric down-conversion (SPDC) and a single-photon nanowire photodetector (SNSPD). One photon of the pair is detected locally, while the other one is sent through a single mode fiber of length  $L$  to be detected on the remote side with Bob's InGaAs avalanche photodiode (APD). Times of arrival for all detected photons are recorded at each side with respect to the local clock, each locked to a rubidium frequency reference (10 MHz). Occasionally, a transmitted photon is reflected at the end face of the fiber back to Alice, allowing her to determine the round-trip time and derive the absolute offset between the clocks.

45 offset fluctuations with an uncertainty of 88 ps in 100 s, consistent with the intrinsic frequency  
 46 instability between our clocks.

## 47 2. Time synchronization protocol

48 The protocol involves two parties, Alice and Bob, connected by a single mode optical fiber (see  
 49 Fig. 1). Alice has an SPDC source producing photon pairs, one photon is detected locally, while  
 50 the other is sent and detected on the remote side. Occasionally, the transmitted photon undergoes  
 51 Fresnel reflection ( $R \approx 3.5\%$ ) at the end face of the fiber, and is eventually detected by Alice  
 52 instead. Every photodetection event is time tagged according to a local clock which assigns time  
 53 stamps  $t$  and  $t'$  at Alice and Bob, respectively.

54 Photon pairs emerging from SPDC are tightly time-correlated ( $\approx 100$  fs) [10]. Thus, for an  
 55 offset  $\delta$  between the clocks, a propagation time  $\Delta t_{AB}$  from Alice to Bob, and  $\Delta t_{BA}$  in the other  
 56 direction, the second-order correlation function [11]  $G^{(2)}(\tau)$  of the time difference  $\tau = t' - t$   
 57 has a peak at

$$\tau_{AB} = \delta + \Delta t_{AB} \quad (1)$$

58 due to pairs detected at opposite ends of the channel, whereas for two photons detected by Alice  
 59 at  $t$  and  $t + \tau$ , the auto-correlation function  $R(\tau)$  will show a peak at

$$\tau_{AA} = \Delta t_{AB} + \Delta t_{BA}, \quad (2)$$

60 corresponding to the round-trip time of the channel. If the propagation times in the two directions  
 61 are the same,  $\Delta t_{AB} = \Delta t_{BA}$ , the the clock offset can be deduced directly from the positions of the  
 62 two peaks using

$$\delta = \tau_{AB} - \frac{1}{2} \tau_{AA}, \quad (3)$$

63 independently of the propagation time  $\Delta t_{AB}$ . In this way, the protocol is inherently robust against  
 64 symmetric changes in channel propagation times.

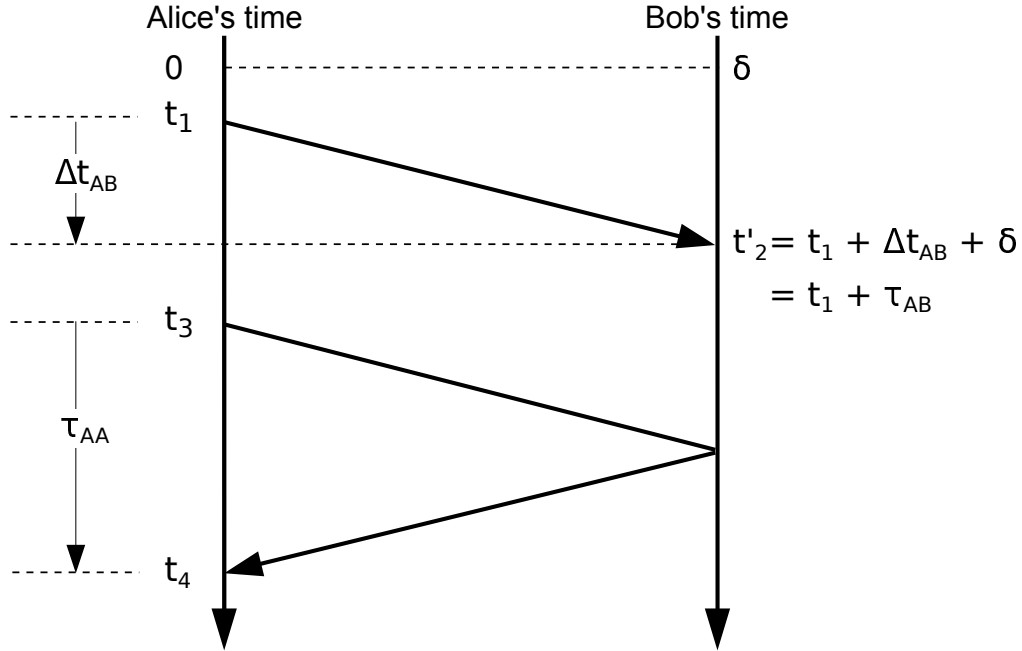


Fig. 2. Clock synchronization scheme. Alice and Bob measure detection times  $t$  and  $t'$  of photon pairs generated from Alice's source using local clocks. Detection times  $t_1$  and  $t'_2$  are associated with a time-correlated photon pair where one photon of the pair is transmitted to Bob, while  $t_3$  and  $t_4$  are associated with a pair where one of the photons is reflected at Bob back to Alice. The single-trip time  $\tau_{AB}$  of photons in the synchronization channel, calculated from the time difference  $t'_2 - t_1$ , depends on the signal delay  $\Delta t_{AB}$  associated with the length of the channel, and the absolute clock offset  $\delta$  between the clocks. The round-trip time  $\tau_{AA}$  of the channel is estimated using  $t_4 - t_3$ . Assuming a symmetric delay channel,  $\delta$  can be derived from  $\tau_{AB}$  and  $\tau_{AA}$  without *a priori* knowing  $\Delta t_{AB}$ .

### 65 3. Experiment

66 A sketch of the experimental setup is shown in Fig. 1. Our photon pair source [12–14] is based  
 67 on Type-0 SPDC in a periodically-poled crystal of potassium titanyl phosphate (PPKTP) pumped  
 68 by a laser diode at 658 nm (Ondax, stabilized with holographic grating). The resulting photon  
 69 pairs are degenerate at 1316 nm, close to the zero dispersion wavelength of the synchronization  
 70 channel (SMF-28e, 10 km), with a bandwidth of  $\approx 50$  nm on either side of this wavelength [14].  
 71 Signal and idler photons are efficiently separated using a wavelength division demultiplexer  
 72 (WDM). Fiber beam splitters separate the photon pairs so that one photon is detected locally  
 73 with a superconducting nanowire single-photon detector (SNSPD, optimized for 1550 nm), while  
 74 the other photon is routed into the synchronization channel where it is detected on the remote  
 75 side with an InGaAs avalanche photodiode (APD). The SNSPD has relatively low jitter ( $\approx 40$  ps)  
 76 compared to APDs ( $\approx 300$  ps), and allows Alice to measure the round-trip time more accurately  
 77 regardless of the choice of detector by the remote party. With a pump power of 2.5 mW focused  
 78 to a beam waist of  $140 \mu\text{m}$  at the centre of the crystal, we observed pair rates of  $160 \text{ s}^{-1}$  and  
 79  $8900 \text{ s}^{-1}$  associated with the round-trip and single-trip propagation of photons, respectively.

80 Photon detection times  $t$  and  $t'$  at Alice and Bob are registered with a nominal resolution of  
 81  $\approx 4$  ps. We compute [15] the histograms  $G^{(2)}(\tau)$  and  $R(\tau)$  with a bin width of of 62.5 ps, and

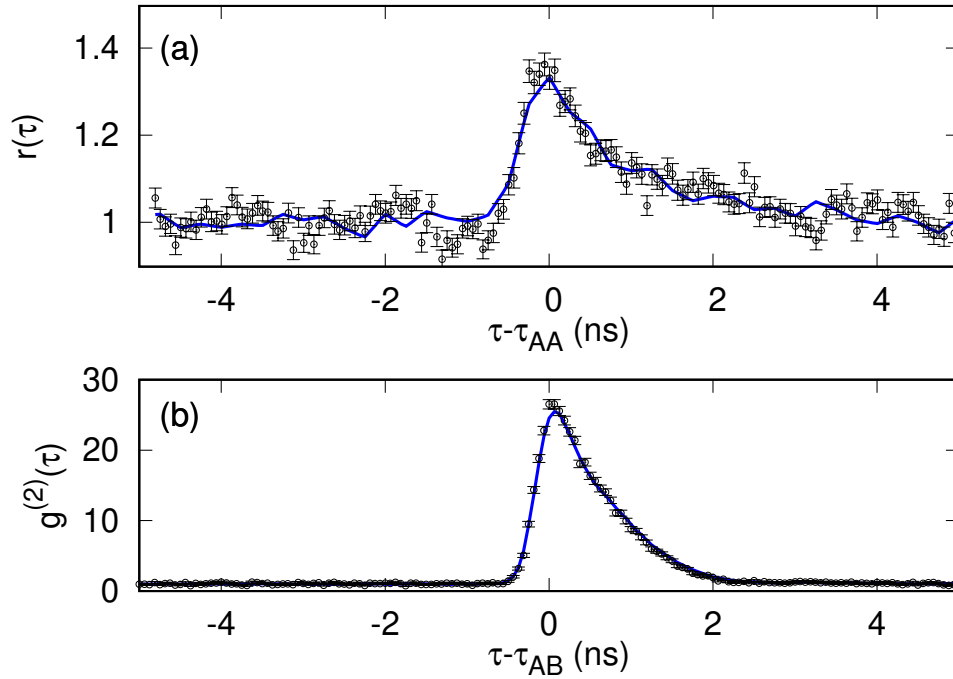


Fig. 3. Timing correlations showing coincidence peaks due to (a) round-trip and (b) single-trip propagation of photons in the synchronization channel. (a)  $r(\tau)$ : auto-correlation function  $R(\tau)$  normalized to background coincidences extracted from Alice's timestamps acquired over 100 s. (b)  $g^{(2)}(\tau)$ : cross-correlation function  $G^{(2)}(\tau)$  normalized to background coincidences extracted from Alice and Bob's timestamps acquired over 3 s. Solid lines: fits to heuristic model.  $\tau_{AA}$  and  $\tau_{AB}$ : peak positions of respective distributions. Error bars: propagated Poissonian counting statistics.

82 observed coincidence peaks associated with the single-trip and round-trip propagating photons  
 83 (FWHM = 905 ps and 950 ps, respectively). Figure 3 shows the respective histograms normalized  
 84 to background coincidences when the two clocks are locked to a common rubidium frequency  
 85 reference (Stanford Research Systems FS725), separated by a fiber spool of constant length  
 86  $L = 10$  km. To deduce the clock offset, we first generate empirical models (Fig. 3, solid-lines)  
 87 for the two coincidence peaks using 100 s of timestamp data – the models are used to fit subsequent  
 88 histograms to extract peak positions  $\tau_{AB}$  and  $\tau_{AA}$ . With the peak positions, we then determine  
 89 the clock offset using Eqs. 2 and 3.

90 To characterize the synchronization precision  $\delta t$  as a function of the acquisition time, we  
 91 measure the standard deviation of twenty offset measurements, each extracted from time stamps  
 92 recorded for a duration  $T_a$ . Figure 4 shows the precision of the measured offset, single-trip  
 93 ( $\tau_{AB}$ ) and round-trip times ( $\tau_{AA}$ ). We observe that the precision for the single and round-trip  
 94 times improves with  $T_a$  for timescales  $\lesssim 100$  s, but deteriorates for longer timescales. We  
 95 attribute this effect to temperature-dependent ( $\Delta T = 45$  mK over 1 min, 160 mK over 3 hours)  
 96 length fluctuations, given that the propagation delay variation [16] of our fiber is several  
 97  $10 \text{ ps km}^{-1} \text{ K}^{-1}$ . However, we observe that these long-term fluctuations are suppressed in the  
 98 clock offset measurement with the distance-independent synchronization protocol.

99 For subsequent demonstrations, we set  $T_a = 3$  s and 90 s for the single and round-trip time

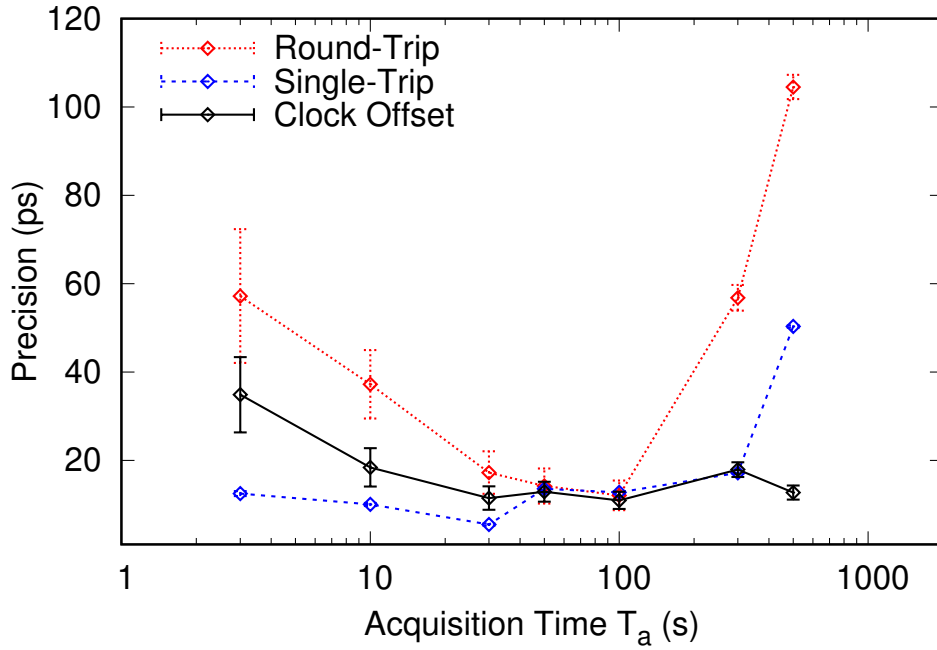


Fig. 4. Precision of the round-trip (red) and single-trip (blue) times, and the clock offset (black) between two clocks. Both clocks are locked to the same frequency reference. Error bars: precision uncertainty due to errors in determining the positions,  $\tau_{AB}$  and  $\tau_{AA}$ , of the coincidence peaks.

100 measurements, obtaining a precision of 12 ps and 14 ps, respectively. Each 90 s window used  
 101 to evaluate the round-trip time thus contains thirty single-trip time measurements. For each  
 102 single-trip time value, we evaluate the clock offset using the round-trip time evaluated in the same  
 103 window. This results in a precision of 16 ps for the measured offset. Measuring the single-trip  
 104 delay with shorter  $T_a$  enables frequent measuring of  $G^{(2)}(\tau)$ , and is useful for tracking the  
 105 position of its coincidence peak ( $\tau_{AB}$ ) in the scenario where clocks are locked to independent  
 106 frequency references.

107 The minimum resolvable clock separation associated with the offset precision is 3.3 mm. To  
 108 demonstrate that the protocol is secure against symmetric channel delay attacks, we change the  
 109 propagation length over several meters during synchronization — three orders of magnitude  
 110 larger than the minimum resolvable length-scale.

#### 111 4. Distance-independent clock synchronization with the same reference clock

112 To simulate a symmetric channel delay attack, we impose different propagation distances using  
 113 different fiber lengths. Figure 5 shows the measured offset  $\delta$  and the round-trip time  $\Delta T$ , with  
 114 an overall standard deviation of 26 ps, and an overall mean of  $\bar{\delta}$ . The sets of  $\delta$  obtained for  
 115  $L = L_0 + 1$  m and  $L_0 + 10$  m, with mean offsets  $\bar{\delta} - 24(17)$  ps, and  $\bar{\delta} + 20(20)$  ps, respectively,  
 116 show significant overlap with those obtained with  $L = L_0 = 10$  km with mean offset  $\bar{\delta} + 1(17)$  ps.  
 117 Comparing the additional mean offset of 19(26) ps to the additional single-trip delay (48.3 ns)  
 118 expected for extending our optical channel from  $L = L_0$  to  $L_0 + 10$  m, our protocol suppresses the  
 119 contribution of the additional propagation delay on the measured offset by a factor of  $\approx 4 \times 10^{-4}$ .

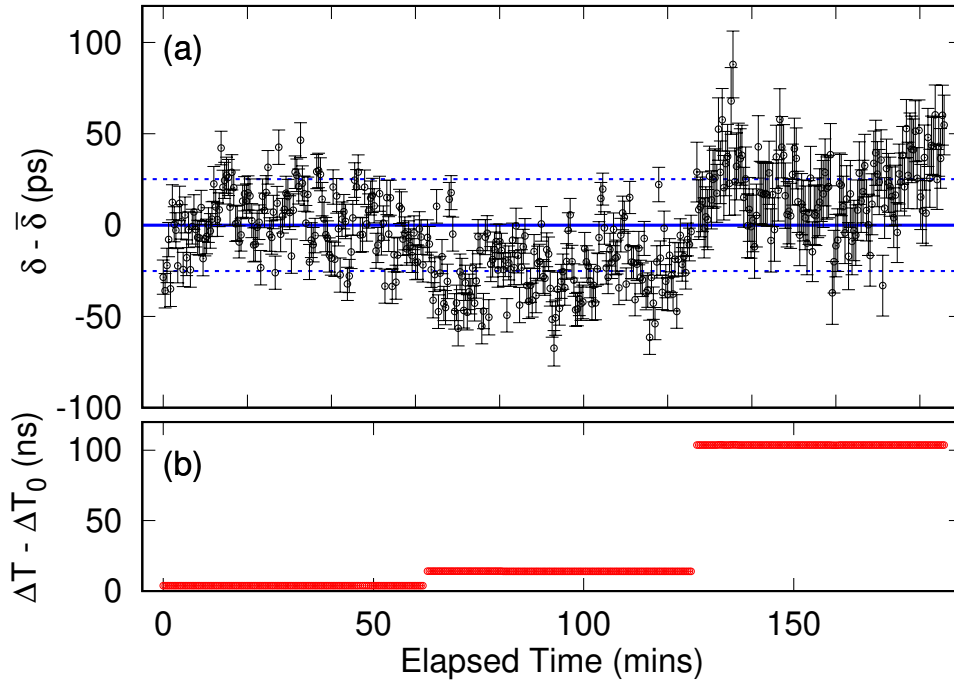


Fig. 5. (a) Measured offset  $\delta$  between two clocks, both locked on the same frequency reference. The continuous line indicates the average offset  $\bar{\delta}$ . Error bars: precision uncertainty due to errors in determining the positions,  $\tau_{AB}$  and  $\tau_{AA}$ , of the coincidence peaks. Dashed lines: one standard deviation. (b) The round-trip time  $\Delta T$  was changed using fiber lengths  $L = L_0 = 10$  km,  $L_0 + 1$  m, and  $L_0 + 10$  m.  $\Delta T_0 = 103.3 \mu\text{s}$ .

120 As the mean offset values do not appear to correlate with  $L$ , we do not attribute the differences  
 121 between the mean offset values to any length-dependent mechanism. We observe however,  
 122 in Fig. 5(a), that the offsets measured changed continuously and gradually even when  $L$  was  
 123 changed abruptly during the the symmetric delay attack. Given these observations, and given  
 124 that both timestamp units were disciplined to the same Rubidium oscillator over the entire  
 125 measurement duration in Fig. 5, it is plausible that the remaining continuous offset drift can  
 126 be attributed to the long-term instability of the timestamp units; the timestamp unit accuracy  
 127 fluctuates due to the non-uniformity of implementing timestamping bin-widths, and varies as a  
 128 function of operation time and temperature.

## 129 5. Distance-independent clock synchronization with independent clocks

130 To examine a more realistic scenario, we provide each time-stamping unit with an independent  
 131 frequency reference (both Stanford Research Systems FS725), resulting in a clock offset that  
 132 drifts with time  $\delta \rightarrow \delta(t)$ .

133 The frequency references each have a nominal frequency accuracy  $d_0 < 5 \times 10^{-11}$ , resulting in  
 134 a relative accuracy  $\sqrt{2} d_0$  between two clocks. We evaluate the offset from the time stamps every  
 135  $T_a = 3$  s so that the maximum expected drift ( $< 212$  ps) of the coincidence peak in  $G^{(2)}(\tau)$  is  
 136 smaller than its FWHM. This pseudo-stationary regime allows the peak positions to be extracted  
 137 with the same fitting procedure used when the clocks are locked onto the same frequency  
 138 reference [6].

139 We again simulate a symmetric channel delay attack using three different values of  $L$ . Figure 6

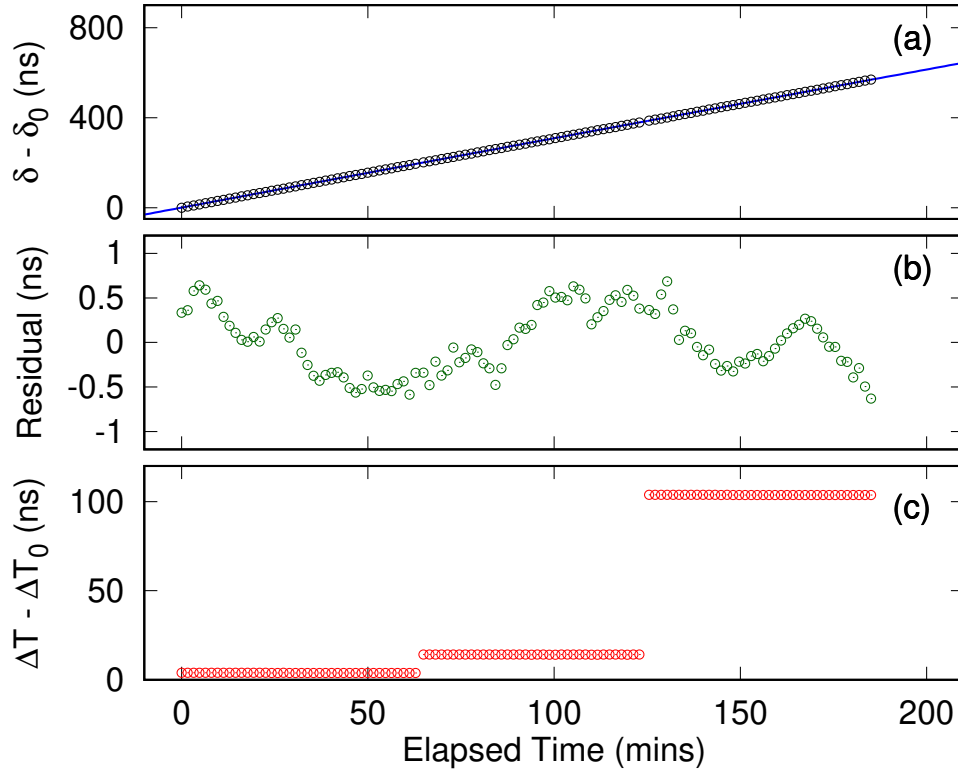


Fig. 6. (a) Measured offset  $\delta$  between two clocks with different frequency references. Each value of  $\delta$  was evaluated from measuring photon pair timing correlations for 3 s. The offset measured at the beginning is  $\delta_0$ . Continuous blue line: fit used to extract the relative frequency accuracy ( $\approx 5.16 \times 10^{-11}$ ) between the clocks. (b) Residual of the fit fluctuates due to the intrinsic instability of the individual frequency references. (c) The round-trip time  $\Delta T$  was changed using three different fiber lengths.

140 shows the measured  $\delta(t)$  which appears to follow a continuous trend over different round-trip  
 141 times, indicating that the delay attacks were ineffective. Discontinuities in  $\delta(t)$  correspond to  
 142 periods when fibers were changed.

143 To verify that meaningful clock parameters can be extracted from  $\delta(t)$  despite the attack, we  
 144 fit the data to a parabola  $at^2 + dt + b$ , where  $a$ ,  $d$  and  $b$  represent the relative aging, frequency  
 145 accuracy and bias of the frequency references, respectively [17]. The resulting relative frequency  
 146 accuracy between the clocks,  $d = 5.1654(7) \times 10^{-11}$ , agrees with the nominal relative frequency  
 147 accuracy  $\sqrt{2}d_0$  between our frequency references. The residual of the fit,  $r(t)$  (Fig. 6(b)),  
 148 fluctuates [18] (Allan deviation =  $2.2 \times 10^{-12}$ , time deviation = 88 ps in 100 s) mainly due to the  
 149 intrinsic instabilities of our frequency references ( $2 \times 10^{-12}$  in 100 s each).

150 The symmetric channel delay attack demonstrated in this work abruptly changed the channel  
 151 length, and is similar to the attacks demonstrated in Refs. [6, 8, 19]. For scenarios where  
 152 the channel delay is changing continuously in time, our protocol is robust against small length  
 153 changes due to thermal fluctuations or mechanical vibrations. To extract the peak positions of the  
 154 cross-correlation and auto-correlation distributions, we need to remain in the pseudo-stationary  
 155 regime where we require that the peaks do not shift significantly compared to their widths.

The upper bound to the rate  $v$  at which the channel length changes is determined by two inequalities:  $\frac{vT_a^{AB}}{\mu} + \sqrt{2}d_0T_a^{AB} < \text{FWHM}^{AB}$  and  $2\frac{vT_a^{AA}}{\mu} < \text{FWHM}^{AA}$ , where  $T_a^{AB}$ ,  $\text{FWHM}^{AB}$  and  $\frac{vT_a^{AB}}{\mu}$  ( $T_a^{AA}$ ,  $\text{FWHM}^{AA}$  and  $2\frac{vT_a^{AA}}{\mu}$ ) is the acquisition time, width and timing-shift of the cross (auto)-correlation coincidence peak,  $\sqrt{2}d_0T_a^{AB}$  the timing-shift due to the relative frequency inaccuracy between the clocks, and  $\mu = 2.04 \times 10^8 \text{ ms}^{-1}$  the speed of 1316 nm photons in the SMF28e fibre. Substituting the values of  $\text{FWHM}^{AB} = 905 \text{ ps}$ ,  $\text{FWHM}^{AA} = 950 \text{ ps}$ ,  $T_a^{AB} = 3 \text{ s}$  and  $T_a^{AA} = 90 \text{ s}$ , we obtain an upper bound of  $v_{max} \approx 50 \text{ mms}^{-1}$  and  $1 \text{ mms}^{-1}$  for measuring the single and round-trip times. We note that this upper bound increases with reduced acquisition times, at the expense of synchronization precision.

## 6. Protocol Security

Although not demonstrated in this work, Alice and Bob can verify the origin of each photon by synchronizing with polarization-entangled photon pairs and performing a Bell measurement to check for correspondence between the local and transmitted photons. This proposal addresses the issue of spoofing in current classical synchronization protocols [6, 7]. **However, due to Presently, classical protocols are unable to authenticate a synchronization signal that has been delayed during an intercept, delay and resend attack when the resent signal has the same cryptographic characteristics as that of the genuine signal [5].** However, when entangled photons are used for synchronization, the same attack will, in-principle, degrade the distributed entanglement and alter the associated Bell measurement. This is a consequence of the quantum no-cloning theorem, which precludes an adversary from making an exact copy of the polarization state of the intercepted photon [20].

Due to the low coincidence-to-accidental ratio associated with the round-trip time measurement (CAR=0.13), this authentication scheme is only feasible for the single-trip time measurement (CAR=8.9). Consequently, users can only authenticate photons traveling from Alice to Bob, and have to assume that the synchronization channel has not been asymmetrically manipulated in order to incorporate the round-trip time measurement in the clock offset calculation (Eqn. 3).

In addition, we also assumed that the photon propagation times in both directions were equal ( $\Delta t_{AB} = \Delta t_{BA}$ ). Without this assumption, the offset

$$\delta = \tau_{AB} - \tau_{AA} + \Delta t_{BA} \quad (4)$$

can no longer be obtained directly from the peak positions  $\tau_{AB}$  and  $\tau_{AA}$ .

We note that an adversary will be able to exploit both assumptions while evading detection by passively rerouting photons traveling in opposite directions in the synchronization channel without disturbing their polarization states [19]. This attack is based on the fact that the momentum and polarization degree-of-freedom of our photons are separable, and remains a security loophole in similar implementations ~~[?,6]~~ [6, 8].

## 7. Conclusion

We have demonstrated a protocol for synchronizing two spatially separated clocks absolutely with time-correlated photon pairs generated from SPDC. By assuming symmetry in the synchronization channel, the protocol does not require *a priori* knowledge of the relative distance or propagation times between two parties, providing security against symmetric channel delay attacks and timing signal authentication via the measurement of a Bell inequality [7]. Compared to previous implementations ~~[?,6]~~ [6, 8], our protocol requires only a single photon pair source, relying on the back-reflected photon to sample the round-trip time of the synchronization channel. This arrangement allows multiple parties to synchronize with bidirectional signals with a single source.

With our protocol, we synchronize two independent rubidium clocks while changing their relative separation, using telecommunication fibers of various lengths ( $\geq 10 \text{ km}$ ) as a synchronization

channel. Even with relatively modest detected coincidence rates ( $160 \text{ s}^{-1}$ ) used for the round-trip time measurement, we obtained a precision sufficient to resolve clock offset fluctuations with a time deviation of 88 ps in 100 s, consistent with the intrinsic frequency instabilities of our clocks. The precision improves with detectors with lower timing jitter [8], brighter sources, or for a transmission channel with insignificant dispersion (free space). Frequency entanglement may also be leveraged to cancel dispersion non-locally, improving protocol precision over optical channels in future work [8].

## 8. Backmatter

**Funding.** This research is supported by the National Research Foundation, Prime Minister's Office, Singapore and the Ministry of Education, Singapore under the Research Centres of Excellence programme.

**Acknowledgments.** We thank S-Fifteen Instruments for assistance with the entangled photon pair source and the InGaAs detector.

**Disclosures.** The authors declare no conflicts of interest.

**Data availability.** Data underlying the results presented in this paper are not publicly available at this time due to their large file size (about 310 Gb) but may be obtained from the authors upon reasonable request.

## References

1. W. Wenjun, D. Shaowu, L. Huanxin, and Z. Hong, "Two-way satellite time and frequency transfer: Overview, recent developments and application," in *2014 European Frequency and Time Forum (EFTF)*, (IEEE, 2014), pp. 121–125.
2. D. L. Mills, "Internet time synchronization: the network time protocol," *IEEE Transactions on Commun.* **39**, 1482–1493 (1991).
3. "Ieee standard for a precision clock synchronization protocol for networked measurement and control systems," IEC 61588:2009(E) pp. C1–274 (2009).
4. P. Moreira, J. Serrano, T. Wlostowski, P. Loschmidt, and G. Gaderer, "White rabbit: Sub-nanosecond timing distribution over ethernet," in *2009 International Symposium on Precision Clock Synchronization for Measurement, Control and Communication*, (2009), pp. 1–5.
5. L. Narula and T. E. Humphreys, "Requirements for secure clock synchronization," *IEEE J. Sel. Top. Signal Process.* **12**, 749–762 (2018).
6. J. Lee, L. Shen, A. Cerè, J. Troupe, A. Lamas-Linares, and C. Kurtsiefer, "Symmetrical clock synchronization with time-correlated photon pairs," *Appl. Phys. Lett.* **114**, 101102 (2019).
7. A. Lamas-Linares and J. Troupe, "Secure quantum clock synchronization," in *Advances in Photonics of Quantum Computing, Memory, and Communication XI*, vol. 10547 (International Society for Optics and Photonics, 2018), p. 105470L.
8. F. Hou, R. Quan, R. Dong, X. Xiang, B. Li, T. Liu, X. Yang, H. Li, L. You, Z. Wang *et al.*, "Fiber-optic two-way quantum time transfer with frequency-entangled pulses," *Phys. Rev. A* **100**, 023849 (2019).
9. R. Quan, H. Hong, W. Xue, H. Quan, W. Zhao, X. Xiang, Y. Liu, M. Cao, T. Liu, S. Zhang *et al.*, "Implementation of field two-way quantum synchronization of distant clocks across a 7 km deployed fiber link," arXiv preprint arXiv:2109.00784 (2021).
10. C.-K. Hong, Z.-Y. Ou, and L. Mandel, "Measurement of subpicosecond time intervals between two photons by interference," *Phys. review letters* **59**, 2044 (1987).
11. R. J. Glauber, "The quantum theory of optical coherence," *Phys. Rev.* **130**, 2529 (1963).
12. Y. Shi, S. M. Thar, H. S. Poh, J. A. Grieve, C. Kurtsiefer, and A. Ling, "Stable polarization entanglement based quantum key distribution over metropolitan fibre network," arXiv preprint arXiv:2007.01989 (2020).
13. A. Lohrmann, C. Perumangatt, A. Villar, and A. Ling, "Broadband pumped polarization entangled photon-pair source in a linear beam displacement interferometer," *Appl. Phys. Lett.* **116**, 021101 (2020).
14. J. A. Grieve, Y. Shi, H. S. Poh, C. Kurtsiefer, and A. Ling, "Characterizing nonlocal dispersion compensation in deployed telecommunications fiber," *Appl. Phys. Lett.* **114**, 131106 (2019).
15. C. Ho, A. Lamas-Linares, and C. Kurtsiefer, "Clock synchronization by remote detection of correlated photon pairs," *New J. Phys.* **11**, 045011 (2009).
16. M. Bousonville and J. Rausch, "Velocity of signal delay changes in fibre optic cables," in *Proceedings of the Ninth European Workshop on Beam Diagnostics and Instrumentation for Particle Accelerators (DIPAC)*, (2009).
17. G. Xu and Y. Xu, *GPS, Theory, Algorithms and Applications* (Springer Berlin Heidelberg, Berlin, Heidelberg, 2016).
18. W. J. Riley, *Handbook of frequency stability analysis* (US Department of Commerce, National Institute of Standards and Technology, 2008).
19. J. Lee, L. Shen, A. Cerè, J. Troupe, A. Lamas-Linares, and C. Kurtsiefer, "Asymmetric delay attack on an entanglement-based bidirectional clock synchronization protocol," *Appl. Phys. Lett.* **115**, 141101 (2019).

- 256 20. W. K. Wootters and W. H. Zurek, "A single quantum cannot be cloned," *Nature* **299**, 802–803 (1982).